arXiv:1704.00435v2 [cond-mat.mtrl-sci] 13 Apr 2017

Thickness-dependent Kapitza resistance in multilayered graphene and other two-dimensional crystals

Zhun-Yong Ong*
*Institute of High Performance Computing, A*STAR, Singapore 138632, Singapore*

The Kapitza or thermal boundary resistance (TBR), which limits heat dissipation from a thin film to its substrate, is a major factor in the thermal management of ultrathin nanoelectronic devices and is widely assumed to be a property of only the interface. However, data from experiments and molecular dynamics simulations suggest that the TBR between a multilayer two-dimensional (2D) crystal and its substrate decreases with increasing film thickness. To explain this thickness dependence, we generalize the recent theory for single-layer 2D crystals by Z.-Y. Ong *et al.* [Phys. Rev. B 94, 165427 (2016)], which is derived from the theory by B. N. J. Persson *et al.* [J. Phys.: Condens. Matter 23, 045009 (2011)], and use it to evaluate the TBR between bare N-layer graphene and SiO_2. Our calculations reproduce quantitatively the TBR thickness dependence seen in experiments and simulations as well as its asymptotic convergence, and predict that the low-temperature TBR scales as T^{-4} in few-layer graphene. Analysis of the interfacial transmission coefficient spectrum shows that the TBR reduction in few-layer graphene is due to the additional contribution from higher flexural phonon branches. Our theory sheds light on the role of flexural phonons in substrate-directed heat dissipation and provides the framework for optimizing the thermal management of multilayered 2D devices.

I. INTRODUCTION

The Kapitza or thermal boundary resistance [1] (TBR) $R_{\rm K}$ between a two-dimensional (2D) crystal (e.g. graphene) and its substrate (e.g. SiO_2) determines the ratio of the temperature difference at the interface (ΔT) to the rate of phonon-mediated heat transfer from the 2D crystal to the substrate (Q), i.e. $R_{\rm K} = \Delta T/Q$, and thus plays a key role in the control of heat dissipation from atomically thin nanoelectronic devices [2–7]. In particular, the lattice thermal boundary conductance (TBC) G, defined as $G = R_{\rm K}^{-1}$, depends on the lattice properties of the materials as well as their van der Waals (vdW) interaction. Although variations in the Kapitza resistance have been attributed [8–11] to differences in interfacial roughness and contact as well as to remote phonon scattering [12, 13], there is increasing evidence from molecular dynamics (MD) simulations [14–19] and experiments [20–23] that the TBR between an unencapsulated or *bare* thin film and its substrate has a strong thickness dependence for which we have no satisfactory explanation especially in a layered crystal such as graphene. It has been observed [14] that the TBR for few-layer graphene decreases significantly as the film thickness (or the number of layers N) increases and asymptotically converges to a fixed value when N is large. This implies that single or few-layer 2D crystals are less efficient at dissipating heat to the substrate and must be factored into the design of high-power nanoelectronic devices.

However, elucidating the physics underlying this TBR thickness dependence is a challenge given the awkwardness of describing *single-sided* cross-plane phonon transport in few-layer films using traditional mismatch models [1] when the two media are dimensionally different [24]. Although MD simulations can reproduce the room-temperature TBR [14, 18], they are computationally expensive, restricted to the classical regime and constrained by size effects [16], and thus they lack direct insight into more fundamental phononic processes. On the other hand, an analytical approach in which flexural phonons are explicitly treated like in Refs. [10, 25] can shed more light on this thickness dependence by yielding new insights into how the layered geometry and individual flexural phonon branches affect interfacial heat dissipation, and thereby improve the control of heat dissipation in layered films such as vdW heterostructures [26]. The continuum physics-based approach to investigating nanoscale interfacial heat dissipation was first formulated by Persson and co-workers and applied to the graphene/SiO_2 interface in Refs. [9, 10, 27] although their predicted TBR values are an order of magnitude too large because of spurious singularities from the use of the weak-coupling approximation. This treatment is refined in Ref. [25] where it is shown that the interfacial heat transport theory can be reformulated into a more conventional Landauer form with a well-defined transmission coefficient spectrum and that flexural phonon damping is necessary to yield a *finite* TBR for single-layer graphene. In addition, the extended treatment enables us to consider the effects of a *superstrate*, such as a top SiO_2 layer, on the TBR, yielding the insight that there is significant distinction between the TBR of a bare 2D crystal and that of a SiO_2-encased sample. In Ref. [25], the calculated TBR values for bare and SiO_2-encased single-layer graphene [25] are in good agreement with experiments and show that the incorporation of the SiO_2 superstrate results in a substantial reduction of the TBR because of the enhanced cross-plane phonon transmission.

In this work, we extend this continuum physics-based

* ongzy@ihpc.a-star.edu.sg

approach by generalizing our recently developed theory of cross-plane substrate-directed heat dissipation for *bare* single-layer 2D crystals [25] to *bare* N-layer 2D crystals and applying it to the graphene/SiO_2 interface. This generalization is essentially made by deriving the Green's function for the flexural motion of the thermally active bottommost sheet in an N-layer stack, as given in Eq. (9), to obtain the correct expression for the interfacial transmission coefficient function [Eq. (2)] needed for calculating the thermal boundary conductance. The additional layers stacked on the bottommost sheet in the N-layer stack modify its flexural response to the interfacial stress exerted by the substrate and, as we shall show later, introduce new transmission channels associated with the higher flexural phonon branches.

Our objectives here are twofold: the first is to elaborate on the theoretical techniques and concepts introduced in Ref. [25] to investigate cross-plane heat dissipation from a 2D crystal and the second is to explain the thickness-dependent TBR seen in Refs. [14–23]. We thus limit the scope of our discussion to *bare* 2D crystals, *i.e.*, multilayer structures without any superstrate such as a top SiO_2 layer, in order to understand more precisely the origin of the TBR difference between single and multilayer 2D crystals. We do not discuss the Kapitza resistance for *encased* multilayer 2D crystals where there is an additional semi-infinite oxide or metal superstrate encapsulating the N-layer 2D crystal because the superstrate also alters the flexural response of the bottommost sheet in contact with the substrate and exerts a similar effect on the interfacial transmission through the introduction of additional transmission channels [25]. Hence, the theory presented in this work does not apply to the configuration in which there is a multilayer 2D crystal sandwiched between two solid slabs like in Refs. [28, 29].

The organization of our paper is as follows. In Sec. II, we begin with a review of the basic theoretical framework established in Ref. [25] for describing flexural phonon-mediated heat dissipation from a one-layer 2D crystal to its substrate. We then show through the derivation of Eqs. (9) and (10) how the theory can be generalized for a bare N-layer 2D crystal or van der Waals heterostructure in which the flexural property of the thermally active bottommost layer is modified by the layers stacked on top of it. In Sec. III, the theory is applied to the study of the TBR of the N-layer graphene/SiO_2 interface and reproduces the TBR reduction observed in thicker graphene samples which we attribute to enhanced interfacial phonon transmission. Our analysis of the transmission coefficient spectra shows that the enhanced transmission and the reduced TBR are due to the more efficient transmission of the higher-frequency flexural phonon branches present in N-layer graphene. We also show that the TBR converges asymptotically as expected when $N \to \infty$, giving us the projected TBR of the graphite/SiO_2 interface. The theoretical concepts and techniques presented in this work are expected to be useful for the analysis and interpretation of the TBR of multilayered structures such as few-layer graphene and van der Waals heterostructures [30].

II. THEORY

A. Basic framework for one-layer 2D crystals

To describe mathematically heat dissipation from a multilayer 2D crystal, we build on the framework introduced in Ref. [25]. The TBC between a single-layer 2D crystal and its substrate [see Fig. 1(a)] is expressed in the Landauer form as [25]

$$G(T) = \frac{1}{(2\pi)^3}\int d^2q \int_0^\infty d\omega \hbar\omega \frac{\partial f(\omega,T)}{\partial T}\Xi(\mathbf{q},\omega)\ , \quad (1)$$

where $f(\omega,T) = [\exp(\hbar\omega/k_BT)-1]^{-1}$ is the Bose-Einstein distribution function at frequency ω and temperature T. The spectrum of the interfacial *transmission coefficient* function $\Xi(\mathbf{q},\omega)$, where

$$\Xi(\mathbf{q},\omega) = \frac{4K^2 \mathrm{Im}D_{\mathrm{sub}}(\mathbf{q},\omega)\mathrm{Im}D_{\mathrm{2D}}(\mathbf{q},\omega)}{|1-K[D_{\mathrm{sub}}(\mathbf{q},\omega)+D_{\mathrm{2D}}(\mathbf{q},\omega)]|^2} \quad (2)$$

and $\mathbf{q}$ is the transverse wave vector, provides an intuitive depiction of the phononic contributions to interfacial transmission and satisfies the constraint $0 < \Xi(\mathbf{q},\omega) \leq 1$. In Eq. (2), K is the spring constant per unit area at the interface between the 2D crystal and the substrate while $D_{\mathrm{sub}}(\mathbf{q},\omega)$ and $D_{\mathrm{2D}}(\mathbf{q},\omega)$ are the retarded Green's functions for the substrate surface and the single-layer 2D crystal, respectively, that describe their flexural or out-of-plane displacement response to the interfacial stress $\sigma_{\mathrm{int}}(\mathbf{q},\omega)$. Assuming an isotropic elastic solid substrate, we have [10, 25, 31]

$$D_{\mathrm{sub}}(\mathbf{q},\omega) = \frac{i}{\rho_{\mathrm{sub}}c_T^2}\frac{p_L(\mathbf{q},\omega)}{S(\mathbf{q},\omega)}\left(\frac{\omega}{c_T}\right)^2 \quad (3)$$

where $S(\mathbf{q},\omega) = [(\omega/c_T)^2 - 2q^2]^2 + 4q^2 p_T p_L$, $p_L(\mathbf{q},\omega) = \lim_{\eta\to 0^+}[(\omega/c_L)^2 - q^2 + i\eta]^{1/2}$, $p_T(\mathbf{q},\omega) = \lim_{\eta\to 0^+}[(\omega/c_T)^2 - q^2 + i\eta]^{1/2}$, and c_L, c_T and ρ_{sub} are its longitudinal and transverse velocities, and its mass density per unit volume, respectively.

If the 2D crystal is bare, *i.e.*, it has no superstrate, then $D_{\mathrm{2D}}(\mathbf{q},\omega)$ in Eq. (2) can be written as [25, 32]

$$D_{\mathrm{2D}}(\mathbf{q},\omega) = [\rho\omega^2 + i\rho\gamma\omega - \kappa q^4]^{-1}\ , \quad (4)$$

where ρ, κ and γ are the mass density per unit area, the bending rigidity and the frequency-dependent flexural damping function of the 2D crystal, respectively. On the other hand, if there is a superstrate such as an oxide layer on top of the 2D crystal (*i.e.* the 2D crystal is encased), then we have $D_{\mathrm{2D}}(\mathbf{q},\omega) = \overline{D}_{\mathrm{2D}}(\mathbf{q},\omega)$, where

$$\overline{D}_{\mathrm{2D}}(\mathbf{q},\omega) = [\rho\omega^2 + i\rho\gamma\omega - \kappa q^4 - P(\mathbf{q},\omega)]^{-1} \quad (5)$$

is the retarded Green's function of the encased 2D sheet, $P(\mathbf{q},\omega) = g_{\rm top}[1 - g_{\rm top}D_{\rm top}(\mathbf{q},\omega)]^{-1}$ is the 'self-energy' contribution from coupling to the superstrate, and $g_{\rm top}$ is the spring constant per unit area at the top interface. The function $D_{\rm top}(\mathbf{q},\omega)$ represents the retarded Green's function for the bottom surface of the superstrate *uncoupled to the thermally active 2D crystal sheet immediately beneath it*. For a superstrate that is a semi-infinite isotropic elastic solid [25], $D_{\rm top}(\mathbf{q},\omega)$ has the same functional form as Eq. (3) although the functional form can be different for other superstrates.

B. Generalization to two- and N-layer 2D crystals

To generalize the TBC model in Ref. [25], we first discuss the case for the two-layer crystal [see Fig. 1(b)], which can be a homogeneous material like bilayer graphene or a composite like a graphene/MoS_2 vdW heterostructure [33]. We do not assume that the two layers are identical for the sake of generality. The TBC calculation using Eqs. (1) and (5) requires us to determine $\overline{D}_{\rm 2D}(\mathbf{q},\omega)$ and $D_{\rm top}(\mathbf{q},\omega)$. In our approach, we treat the two-layer system as an encased one-layer 2D crystal, and identify the top layer (sheet 1) as the 'superstrate' and the bottom layer (sheet 2) as the thermally active sheet that dissipates heat to the substrate. Hence, we write $D_{\rm top}(\mathbf{q},\omega) = D^{(1)}_{\rm 2D}(\mathbf{q},\omega)$, where

$$D^{(1)}_{\rm 2D}(\mathbf{q},\omega) = [\rho_1\omega^2 + i\rho_1\gamma_1\omega - \kappa_1 q^4]^{-1} \qquad (6)$$

is the retarded Green's function for the *uncoupled* sheet 1 like in Eq. (4) and ρ_1, γ_1 and κ_1 are the areal mass density, the frequency-dependent flexural damping function and bending rigidity, respectively, for sheet 1. We write the retarded Green's function for the bottom layer (sheet 2), which is coupled to the top layer but uncoupled to the substrate, as $\overline{D}_{\rm 2D}(\mathbf{q},\omega) = D^{(2)}_{\rm 2D}(\mathbf{q},\omega)$, where

$$D^{(2)}_{\rm 2D}(\mathbf{q},\omega) = [\rho_2\omega^2 + i\rho_2\gamma_2\omega - \kappa_2 q^4 - P_2]^{-1}\ , \qquad (7)$$

and

$$P_2(\mathbf{q},\omega) = g_{2,1}[1 - g_{2,1}D^{(1)}_{\rm 2D}(\mathbf{q},\omega)]^{-1} \qquad (8)$$

is the 'self-energy' of sheet 2 from coupling to sheet 1 and corresponds to the change in the flexural response of sheet 2 due to that coupling. The terms ρ_2, γ_2 and κ_2 represent the areal mass density, the frequency-dependent flexural damping function and bending rigidity, respectively, for sheet 2 while $g_{2,1}$ is the spring constant per unit area coupling sheets 1 and 2. Physically, $D^{(2)}_{\rm 2D}(\mathbf{q},\omega)$ is the mechanical transfer function that describes the flexural response of sheet 2 to the interfacial stress exerted on its bottom surface by the substrate.

We make the observation that in the two-layer crystal, $D^{(n)}_{\rm 2D}(\mathbf{q},\omega)$ for $n = 1, 2$ describes the flexural response of sheet n to the interfacial stress exerted from the bottom and, for $n = 2$, includes only the effects of mechanical coupling to the sheet immediately above it via the self-energy term in Eq. (8). Also, the bottom layer (sheet 2) is the thermally active sheet from which heat is dissipated to the substrate. This suggests that for the N-layer crystal where the individual sheets are numbered from 1 (top) to N (bottom) as shown in Fig. 1(c), the flexural response of the thermally active bottom layer (sheet N) is described by the Green's function

$$D^{(N)}_{\rm 2D}(\mathbf{q},\omega) = [\rho_N\omega^2 + i\rho_N\gamma_N\omega - \kappa_N q^4 - P_N]^{-1}\ , \quad (9)$$

where $P_N(\mathbf{q},\omega) = g_{N,N-1}[1 - g_{N,N-1}D^{(N-1)}_{\rm 2D}(\mathbf{q},\omega)]^{-1}$ and $g_{N,N-1}$ is the spring constant per unit area coupling sheets N and $N-1$. In effect, $D^{(N)}_{\rm 2D}(\mathbf{q},\omega)$ depends on $D^{(N-1)}_{\rm 2D}(\mathbf{q},\omega)$ which in turn depends on $D^{(N-2)}_{\rm 2D}(\mathbf{q},\omega)$ and so on. Thus, we can recursively define $D^{(n)}_{\rm 2D}(\mathbf{q},\omega)$ for $n = N, N-1, \ldots, 1$ with $D^{(1)}_{\rm 2D}(\mathbf{q},\omega)$ defined in Eq. (6) describing the flexural response of sheet 1 at the top of the N-layer stack.

In the N-layer 2D crystal composed of identical sheets, we have $\rho_1 = \ldots = \rho_N = \rho$, $\kappa_1 = \ldots = \kappa_N = \kappa$ and $\gamma_1 = \ldots = \gamma_N = \gamma(\omega)$ while the interlayer spring constant per unit area is given by $g_{N,N-1} = \ldots = g_{2,1} = g$, and there are N flexural phonon branches. Therefore, $D^{(N)}_{\rm 2D}(\mathbf{q},\omega)$, the retarded Green's function for the flexural motion of the thermally active bottom sheet, can be expressed as a weighted sum of the contributions by the flexural phonon branches, *i.e.*,

$$D^{(N)}_{\rm 2D}(\mathbf{q},\omega) = \sum_{n=1}^{N} \frac{f_n}{\rho\omega^2 + i\rho\gamma(\omega)\omega - \rho\omega_n^{(N)}(q)^2} \qquad (10)$$

where $f_1 = \frac{1}{N}$ and $f_n = \frac{1}{N}[1 + \cos\frac{(n-1)\pi}{N}]$ for $1 < n \leq N$ are the weights. The details of the derivation of Eq. (10) are given in the Appendix. The term $\omega_n^{(N)}(q)$ describes the phonon dispersion for the n-th branch and is given by

$$\omega_n^{(N)}(q) = \sqrt{\frac{\kappa}{\rho}q^4 + (\Omega_n^{(N)})^2}\ , \qquad (11)$$

where $\Omega_n^{(N)} = \sqrt{\frac{4g}{\rho}}\left|\sin\frac{(n-1)\pi}{2N}\right|$ is the Γ-point ($q = 0$) phonon frequency for the n-th phonon branch in the N-layer 2D crystal [34, 35].

III. RESULTS AND DISCUSSION

A. Dependence of TBR on film thickness and temperature

To evaluate the effectiveness of the theory, we compute $R_{\rm K}$ for the graphene/SiO_2 interface for different N using Eqs. (1) and (10), and plot the results in Fig. 2

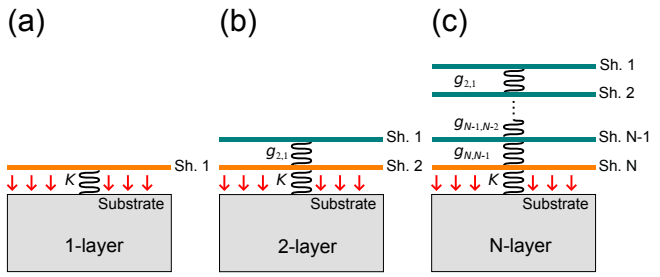

Figure 1. Schematic of the substrate-supported (a) one-layer, (a) two-layer and (c) N-layer 2D crystal. Adjacent sheets are connected to each other by a harmonic force (represented by the springs). In our convention, the individual sheets in the "superstrate" are numbered from 1 to $N-1$ with sheet 1 ('Sh. 1') being the topmost sheet and sheet N ('Sh. N') being the bottommost sheet. Direct interfacial heat transfer occurs only between the thermally active bottom sheet and the substrate.

alongside data from experiments [20] and MD simulations [14] for comparison. The parameters c_L, c_T, $\rho_{\rm sub}$, ρ and κ and the damping function $\gamma(\omega)$ for the flexural motion of individual graphene sheets are taken from Ref. [25] while we set $g = 1.095 \times 10^{20}$ Nm^{-3} which we estimate from the Γ-point interlayer breathing mode frequency ($\omega_B = 11.2$ meV) for bilayer graphene [36] using the formula $g = \frac{1}{2}\rho\omega_B^2$ derived from Eq. (11). In the $N \to \infty$ limit where we have graphite, the frequency spacing between the flexural phonon dispersion curves vanishes and this value of g can be used to estimate c_z the speed of sound in the out-of-plane direction. Our estimate using the expression $c_z = a\sqrt{g/\rho}$, where $a = 0.335$ nm is the interlayer spacing in graphite, yields $c_z = 4021$ ms^{-1}, in excellent agreement with reported values [37].

We also define the effective TBR ($R'_{\rm K}$), which corresponds to the higher thermal resistance due to contact imperfections at the interface [38, 39], as $R'_{\rm K} = R_{\rm K}/\chi$ where $0 < \chi \leq 1$ is the effective contact between graphene and the substrate, and plot $R'_{\rm K}$ for $\chi = 0.72$. Figure 2 shows $R_{\rm K}$ exhibiting a thickness dependence qualitatively similar to the MD simulation data [14]: $R_{\rm K}$ decreases as N increases and converges asymptotically at large N. Quantitative agreement between our theory and the MD simulation data improves when we use $R'_{\rm K}$ instead of $R_{\rm K}$, indicating contact imperfection as a possible cause of discrepancy. Other possible explanations for the discrepancy include: (1) the fact that a continuum theory like ours cannot perfectly describe the dynamics of an atomistic model especially outside the long-wavelength regime, and (2) the variations in the effective elasticity parameters which can lead to differences in the computed TBR values. For instance, the Brenner-type interatomic potentials [40] used in Ref. [14] have been shown [41] to yield a smaller bending rigidity value which corresponds to a lower numerical value for the TBC (or higher $R_{\rm K}$) in our theory. In addition, finite-size effects in MD simulations can be another source of discrepancy.

The $R'_{\rm K}$ values also broadly agree with the experimental data from Ref. [20] although the spread in the experimental values, possibly due to variation in the effective contact of the interface (χ) as well as other experimental factors, makes it difficult for us to fit the data properly. Indeed, the simulated $R_{\rm K}$ curve corresponding to $\chi = 1$ in Fig. 2 sets the lower bound for the range of TBR values extracted from Ref. [20] except at $N = 5$ and 6, suggesting that a significant percentage of the interface may not be in perfect ($\chi = 1$) contact for most samples. Another possible cause of the poor disagreement is the corrugation of the graphene/SiO_2 interface [42] which may introduce stochastic variation in the measured TBR not captured by our theory. Modeling this corrugation effect on the TBR however requires additional modification of our theory and a deeper understanding of the connection between interfacial heat flow and contact mechanics, which is beyond the scope of the current work although it is discussed in Ref. [27]. We also obtain $R'_{\rm K} = 1.14 \times 10^{-8}$ m^{2}KW^{-1} for $N = 100$ which approximates our projection for the effective TBR of the room-temperature graphite/SiO_2 interface. This numerical value is comparable to the room-temperature TBR value ($\sim 10^{-8}$ m^{2}KW^{-1}) obtained by Schmidt and co-workers [43] for the interface between highly ordered pyrolytic graphite (HOPG) and Al film with a 5-nm Ti adhesion layer although such a comparison between this TBR value and our projected effective TBR for the graphite/SiO_2 interface cannot be rigorously made as the substrate materials are different.

Figure 3 also shows the TBR for $N = 1$ to 13 and $T = 20$ to 600 K decreasing with temperature and scaling approximately as $R_{\rm K} \propto T^{-4}$ at low temperatures instead of the typical T^{-3} behavior [1] seen in nonlayered systems [44, 45]. The $R_{\rm K} \propto T^{-4}$ behavior is also noted in Ref. [25] and is attributed to the ω^3 scaling of the total interfacial transmission $\Theta(\omega)$ at low frequencies. At low temperatures ($T \leq 100$ K), the difference in $R_{\rm K}$ for $N = 1$ and $N = 13$ is significantly larger, by almost an order of magnitude, than the difference at high temperatures ($T \geq 300$ K).

B. Dependence of the interfacial transmission spectrum on film thickness

The TBR reduction in thicker samples shown in Fig. 2 can be interpreted in terms of changes in the overall phonon transmission between graphene and the SiO_2 substrate. To quantify the overall phonon transmission, we define the frequency-dependent transmission function per unit area [25]

$$\Theta(\omega) = \frac{1}{(2\pi)^2}\int d^2q \Xi(\mathbf{q},\omega) \ . \qquad (12)$$

Figure 4(a) shows $\Theta(\omega)$ for $N = 1$, 2, 3, 6, 10, 40 and 100, with the $N = 100$ spectrum approximating the graphite/SiO_2 interface. We find that as N increases, the additional layers result in substantial enhancement

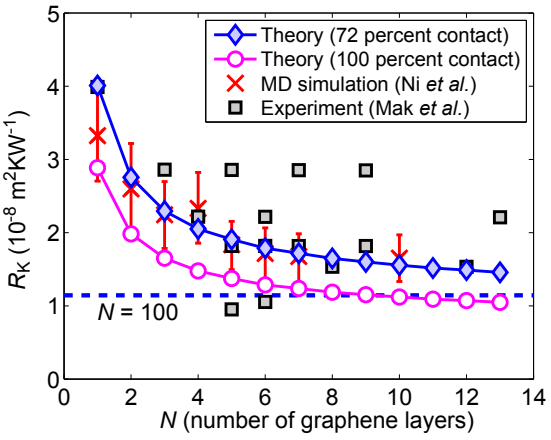
Theory (72 percent contact)
Theory (100 percent contact)
MD simulation (Ni et al.)
Experiment (Mak et al.)
N = 100
R_K (10^-8 m^2KW^-1)
N (number of graphene layers)

Figure 2. Comparison of the theoretical room-temperature thermal boundary resistance ($R_{\rm K}$) vs. number of graphene layers (N) (circles) with data taken from experiments [20] (squares) and MD simulations [14] (cross symbols). We also plot the effective thermal boundary resistance ($R'_{\rm K}$) corresponding to 72 percent contact (diamond symbols). The dashed line (1.14×10^{-8} m^{2}KW^{-1}) corresponds to $R'_{\rm K}$ for $N=100$ and approximates the simulated $R'_{\rm K}$ for the graphite/SiO_2 interface.

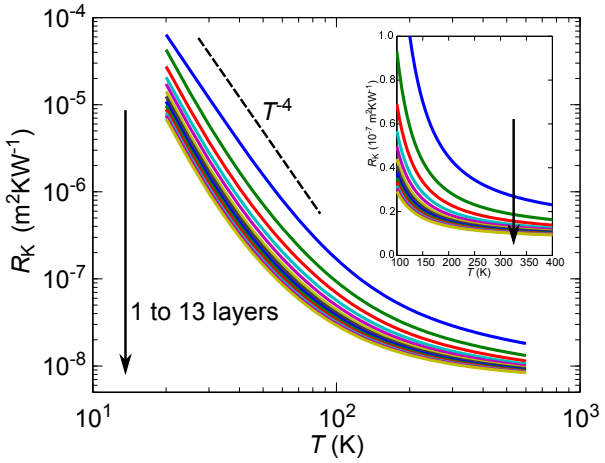

Figure 3. Thermal boundary resistance of the graphene/SiO_2 interface for $N=1$ to 13 and $T=20$ to 600 K. The inset shows the same data from $T=100$ to 400 K with a linear scale.

of $\Theta(\omega)$ especially at lower frequencies. Hence, we attribute the decrease in TBR for few-layer graphene to the progressively enhanced cross-plane transmission of low-frequency modes as N increases. In addition, we also observe a number of peaks in $\Theta(\omega)$ which increases as N gets larger. This can be more clearly seen in the inset of Fig. 4(a) where the smooth $N=1$ spectrum is contrasted with the $N=6$ spectrum with five peaks, of which the higher frequency ones are sharper and more closely spaced. In general, there are $N-1$ peaks in the transmission spectrum of N-layer graphene although the peaks gradually merge together when N is large as is evident from the $N=40$ and 100 spectra which are practically identical for $\omega > 15$ meV.

The origin of the enhanced phonon transmission and the transmission peaks can be connected to the flexural phonon dispersion in N-layer graphene by analyzing the transmission coefficient function $\Xi(\mathbf{q},\omega)$ which we plot for different values of N in Fig. 4(b)-4(g). In one-layer graphene [Fig. 4(b)], the low-q part of the transmission coefficient spectrum corresponding to the only flexural phonon branch is insignificant because the associated phonon frequencies are less than the substrate bulk transverse acoustic frequencies, i.e. $\omega < c_T q$, which results in weak coupling between the low-frequency flexural phonon modes and the substrate as pointed out in Ref. [25] In two-layer graphene [Fig. 4(c)], the lower phonon branch does not contribute significantly to interfacial transmission like in one-layer graphene since $\omega < c_T q$ but the upper phonon branch contribution is more pronounced in the low-q part of the transmission spectrum as the associated upper branch modes satisfy the condition $\omega > c_T q$. The contribution from the higher phonon branches becomes more substantial for three, six and ten-layer graphene [Figs. 4(d)-4(f)]. In particular, the higher phonon branches show sharper transmission peaks, indicating more efficient interfacial transmission. Therefore, we attribute the enhanced cross-plane phonon transmission and hence the lower TBR of a thicker graphene film to the interfacial transmission contribution from its additional flexural phonon branches, which becomes more pronounced for low frequencies and produces the greater low-temperature R_K change with respect to N seen in Fig. 3. Also, the transmission peaks in Fig. 4(a) are due to the long wavelength ($q \to 0$) modes of the $N-1$ higher flexural branches in N-layer graphene.

However, when N is large [e.g., $N=40$ in Fig. 4(g)], the contribution to interfacial transmission becomes much less dependent on N. This can be explained by noting that the transmission coefficient function in Eq. (2) can be expressed as the sum of the transmission by each phonon branch, *i.e.*,

$$\Xi(\mathbf{q},\omega) = \sum_{n=1}^{N} \frac{4K^2 {\rm Im}D_{\rm sub}(\mathbf{q},\omega){\rm Im}D_n(\mathbf{q},\omega)}{|1-K[D_{\rm sub}(\mathbf{q},\omega)+D_{\rm 2D}(\mathbf{q},\omega)]|^2} \quad (13)$$

where $D_n(\mathbf{q},\omega)$ is the summand in Eq. (10) and is proportional to the weight f_n which scales as N^{-1}. Therefore, at large N, the transmission contribution in Eq. (13) by each closely spaced phonon branch scales as N^{-1} and thus, the total transmission and the TBR converge asymptotically with respect to N because the additional transmission contribution from having more phonon branches is canceled out by the diminishing contribution of each branch. This weak N dependence is also evident from the very similar transmission spectra for $N=40$ and 100 in Fig. 4(a).

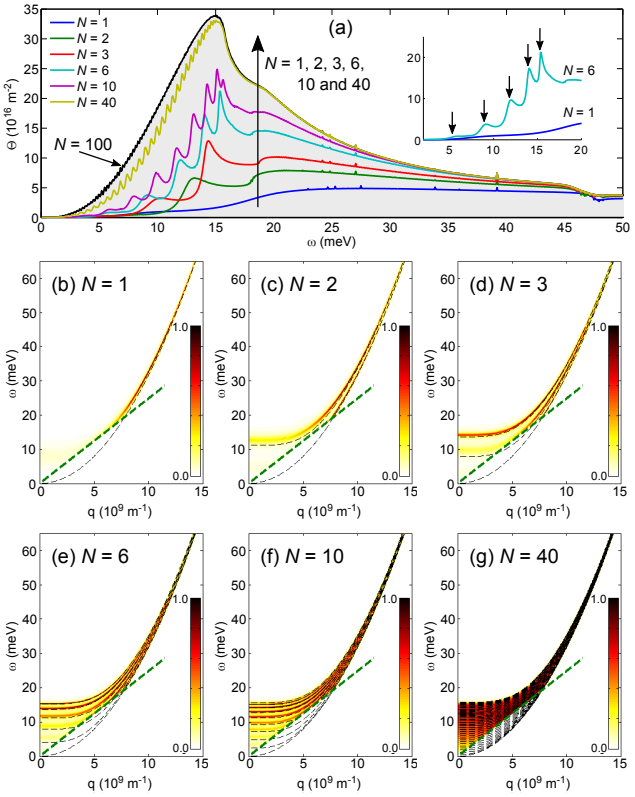

Figure 4. (a) Overall transmission per unit area $\Theta(\omega)$ for $N = 1$, 2, 3, 6, 10, 40 and 100, with the $N = 100$ spectrum (shaded gray) approximating the graphite/SiO_2 spectrum. The inset compares the low-frequency spectra for $N = 1$ and $N = 6$ with peak positions in the latter indicated by arrows. We also plot the transmission coefficient spectrum $\Xi(\mathbf{q}, \omega)$ for (b) 1-, (c) 2-, (d) 3-, (e) 6-, (f) 10-, and (g) 40-layer graphene. The thin black dashed lines correspond to the flexural phonon branch dispersion given by Eq. (11), while the thicker green dashed lines correspond to the bulk transverse acoustic phonon dispersion for the substrate ($\omega = c_T q$).

IV. SUMMARY AND CONCLUSIONS

In summary, we have generalized the theory of heat dissipation in Ref. [25] to multilayer 2D crystals and used it to evaluate the TBR of the graphene/SiO_2 interface for different layer numbers and temperatures. The key idea in the generalization is to treat the top $N-1$ layers in an N-layer stack as a superstrate. The numerical results show that the TBR decreases with N, consistent with what has been observed in MD simulations and experiments, and converges asymptotically to a constant corresponding to the graphite/SiO_2 TBR. Our theory explains (1) the TBR reduction with respect to layer number in terms of the enhanced interfacial transmission contribution by the additional flexural phonon branches and (2) its asymptotic convergence, and predicts a low-temperature $R_K \propto T^{-4}$ behavior. It can also opens up new possibilities of heat dissipation control through modification of the layered structure.

ACKNOWLEDGMENTS

This work was supported in part by a grant from the Science and Engineering Research Council (152-70-00017) and financial support from the Agency for Science, Technology and Research (A*STAR), Singapore.

Appendix: Derivation of $D_{2D}^{(N)}(\mathbf{q}, \omega)$

Here, we derive $D_{2D}^{(N)}(\mathbf{q}, \omega)$ in Eq. (10). The equations of motion for layers 1 to N in the N-layer system can be written as

$$-(\rho\omega^2 + i\rho\gamma\omega - \kappa q^4)u_1 = -g(u_1 - u_2) \ , \qquad \text{(A.1a)}$$

$$-(\rho\omega^2 + i\rho\gamma\omega - \kappa q^4)u_N = -g(u_N - u_{N-1}) \qquad \text{(A.1b)}$$

$$-(\rho\omega^2 + i\rho\gamma\omega - \kappa q^4)u_j = -g(2u_j - u_{j-1} - u_{j+1}) \ , \qquad \text{(A.1c)}$$

where $j = 2, \ldots, N-1$ and $u_l = u_l(\mathbf{q}, \omega)$ is the flexural displacement of the l-th layer. We can express Eq. (A.1) more compactly as an eigenvalue equation

$$\sum_{j=1}^{N}(V_{ij} - z\delta_{ij})u_j = 0 \ , \qquad \text{(A.2)}$$

where $z(\mathbf{q}, \omega) = \rho\omega^2 + i\rho\gamma(\omega)\omega - \kappa q^4$, $V_{ij} = -g(\delta_{i,j-1} + \delta_{i,j+1})$ for $i \neq j$ and $V_{ii} = \sum_{j=1}^{N}(\delta_{ij} - 1)V_{ij}$ for $i = 1, \ldots, N$. The matrix V is an $N \times N$ tridiagonal matrix in which the off-diagonal elements have a value of $-g$ and the diagonal elements are equal to the negative sum of the off-diagonal values in the row. Therefore, the n-th eigenvalue of V in Eq. (A.2) is given by [34] $z_n = 4g\sin^2\left[\frac{(n-1)\pi}{2N}\right]$ while the flexural displacement of the j-th layer for the corresponding n-th normalized eigenvector is

$$u_j^n = \sqrt{\frac{2}{N}}\cos\left[\frac{(n-1)(2j-1)\pi}{2N}\right] \qquad \text{(A.3)}$$

for $n = 2, \ldots, N$ and $u_j^n = 1/\sqrt{N}$ for $n = 1$. The $N \times N$ matrix describing the Green's function of the system can be written as a resolvent, *i.e.*, $G_{ij}(z) = \left(\frac{1}{z-V}\right)_{ij} = \sum_{n=1}^{N}(u_i^n)^\dagger u_j^n (z - z_n)^{-1}$. Thus, the flexural response of the bottommost layer ($j = N$) is

$$D_{2D}^{(N)}(\mathbf{q}, \omega) = G_{NN}(z(\mathbf{q}, \omega)) = \sum_{n=1}^{N}\frac{f_n}{z(\mathbf{q}, \omega) - z_n} \ , \qquad \text{(A.4)}$$

where $f_1 = \frac{1}{N}$ and $f_n = \frac{1}{N}[1 + \cos\frac{(n-1)\pi}{N}]$ for $1 < n \leq N$. In the large N limit, we can write Eq. (A.4) as an integral, *i.e.*,

$$\lim_{N\to\infty} D_{2D}^{(N)}(\mathbf{q}, \omega) = \frac{1}{\pi}\int_0^\pi d\theta \frac{1 + \cos\theta}{z(\mathbf{q}, \omega) - 4g\sin^2(\frac{1}{2}\theta)} \ . \qquad \text{(A.5)}$$

[1] E. T. Swartz and R. O. Pohl, Rev. Mod. Phys. **61**, 605 (1989).
[2] M. Freitag, M. Steiner, Y. Martin, V. Perebeinos, Z. Chen, J. C. Tsang, and P. Avouris, Nano Lett. **9**, 1883 (2009).
[3] E. Pop, Nano Research **3**, 147 (2010).
[4] M.-H. Bae, Z.-Y. Ong, D. Estrada, and E. Pop, Nano Lett. **10**, 4787 (2010).
[5] M.-H. Bae, Z. Li, Z. Aksamija, P. N. Martin, F. Xiong, Z.-Y. Ong, I. Knezevic, and E. Pop, Nature Commun. **4**, 1734 (2013).
[6] A. Y. Serov, Z.-Y. Ong, M. V. Fischetti, and E. Pop, J. Appl. Phys. **116**, 034507 (2014).
[7] D. Li and A. J. H. McGaughey, Nanoscale and Microscale Thermophysical Engineering **19**, 159 (2015).
[8] W. Cai, A. L. Moore, Y. Zhu, X. Li, S. Chen, L. Shi, and R. S. Ruoff, Nano Lett. **10**, 1645 (2010).
[9] B. Persson and H. Ueba, J. Phys.: Condens. Matter **22**, 462201 (2010).
[10] B. N. J. Persson, A. I. Volokitin, and H. Ueba, J. Phys.: Condens. Matter **23**, 045009 (2011).
[11] C. Liu, Z. Wei, J. Wang, K. Bi, J. Yang, and Y. Chen, AIP Advances **5**, 127111 (2015).
[12] Z.-Y. Ong, M. V. Fischetti, A. Y. Serov, and E. Pop, Phys. Rev. B **87**, 195404 (2013).
[13] Y. K. Koh, A. S. Lyons, M.-H. Bae, B. Huang, V. E. Dorgan, D. G. Cahill, and E. Pop, Nano Lett. **16**, 6014 (2016).
[14] Y. Ni, Y. Chalopin, and S. Volz, Appl. Phys. Lett. **103**, 141905 (2013).
[15] Z. Liang, K. Sasikumar, and P. Keblinski, Phys. Rev. Lett. **113**, 065901 (2014).
[16] Z. Liang and P. Keblinski, Phys. Rev. B **90**, 075411 (2014).
[17] J. Chen, J. H. Walther, and P. Koumoutsakos, Nano Lett. **14**, 819 (2014).
[18] Y. Ni, Y. A. Kosevich, S. Xiong, Y. Chalopin, and S. Volz, Phys. Rev. B **89**, 205413 (2014).
[19] D. Alexeev, J. Chen, J. H. Walther, K. P. Giapis, P. Angelikopoulos, and P. Koumoutsakos, Nano Lett. **15**, 5744 (2015).
[20] K. F. Mak, C. H. Lui, and T. F. Heinz, Appl. Phys. Lett. **97**, 221904 (2010).
[21] F. Menges, H. Riel, A. Stemmer, C. Dimitrakopoulos, and B. Gotsmann, Phys. Rev. Lett. **111**, 205901 (2013).
[22] J. Yang, M. Shen, Y. Yang, W. J. Evans, Z. Wei, W. Chen, A. A. Zinn, Y. Chen, R. Prasher, T. T. Xu, P. Keblinski, and D. Li, Phys. Rev. Lett. **112**, 205901 (2014).
[23] P. Yuan, C. Li, S. Xu, J. Liu, and X. Wang, Acta Materialia **122**, 152 (2017).
[24] G. C. Correa, C. J. Foss, and Z. Aksamija, Nanotechnology **28**, 135402 (2017).
[25] Z.-Y. Ong, Y. Cai, and G. Zhang, Phys. Rev. B **94**, 165427 (2016).
[26] K. S. Novoselov, A. Mishchenko, A. Carvalho, and A. H. Castro Neto, Science **353**, 461 (2016).
[27] B. N. J. Persson, B. Lorenz, and A. I. Volokitin, Eur. Phys. J. E **31**, 3 (2010).
[28] H. Zhao and J. Freund, J. Appl. Phys. **97**, 024903 (2005).
[29] M. Shen, P. K. Schelling, and P. Keblinski, Phys. Rev. B **88**, 045444 (2013).
[30] A. K. Geim and I. V. Grigorieva, Nature **499**, 419 (2013).
[31] B. N. J. Persson, J. Chem. Phys. **115**, 3840 (2001).
[32] B. Amorim and F. Guinea, Phys. Rev. B **88**, 115418 (2013).
[33] B. Liu, F. Meng, C. D. Reddy, J. A. Baimova, N. Srikanth, S. V. Dmitriev, and K. Zhou, RSC Adv. **5**, 29193 (2015).
[34] N. S. Luo, P. Ruggerone, and J. P. Toennies, Phys. Rev. B **54**, 5051 (1996).
[35] Y. Zhao, X. Luo, H. Li, J. Zhang, P. T. Araujo, C. K. Gan, J. Wu, H. Zhang, S. Y. Quek, M. S. Dresselhaus, and Q. Xiong, Nano Lett. **13**, 1007 (2013).
[36] J.-A. Yan, W. Y. Ruan, and M. Y. Chou, Phys. Rev. B **77**, 125401 (2008).
[37] R. Prasher, Phys. Rev. B **77**, 075424 (2008).
[38] B. Huang and Y. K. Koh, Carbon **105**, 268 (2016).
[39] Y. Liu, Z.-Y. Ong, J. Wu, Y. Zhao, K. Watanabe, T. Taniguchi, D. Chi, G. Zhang, J. T. Thong, C.-W. Qiu, *et al.*, Scientific Reports **7**, 43886 (2017).
[40] D. W. Brenner, Phys. Rev. B **42**, 9458 (1990).
[41] Q. Lu, M. Arroyo, and R. Huang, J. Phys. D: Appl. Phys. **42**, 102002 (2009).
[42] M. Ishigami, J. H. Chen, W. G. Cullen, M. S. Fuhrer, and E. D. Williams, Nano Lett. **7**, 1643 (2007).
[43] A. J. Schmidt, K. C. Collins, A. J. Minnich, and G. Chen, J. Appl. Phys. **107**, 104907 (2010).
[44] J. Schleeh, J. Mateos, I. I. de-la Torre, N. Wadefalk, P. A. Nilsson, J. Grahn, and A. J. Minnich, Nature Mater. **14**, 187 (2015).
[45] P. Zolotavin, A. Alabastri, P. Nordlander, and D. Natelson, ACS Nano **10**, 6972 (2016).